ELSEVIER

Materials Science and Engineering A273–275 (1999) 738–744

MATERIALS SCIENCE & ENGINEERING A

www.elsevier.com/locate/msea

Structure and properties of Ti–Ni–Zr and Ti–Ni–Hf melt-spun ribbons

E. Cesari [a], P. Ochin [b], R. Portier [b,c], V. Kolomytsev [d,*], Yu. Koval [d], A. Pasko [d], V. Soolshenko [d]

[a] *Departament de Fisica, Universitat de les Illes Balears, Palma de Mallorca, Spain*
[b] *Centre d'Etudes de Chimie Métallurgique, CNRS, Vitry, France*
[c] *Laboratoire de Métallurgie Structurale, Ecole Nationale Supérieure de Chimie de Paris, Paris, France*
[d] *Institute of Metal Physics, National Academy of Sciences of Ukraine, Kiev, Ukraine*

Abstract

Rapidly solidified ribbons of Ti–Ni–Zr and Ti–Ni–Hf shape memory alloys for high-temperature applications have been produced using a planar flow casting technique. Calorimetric and mechanical measurements, as well as transmission electron microscopy (TEM) observations have been performed. The characteristics of martensitic transformation in the ribbons are studied and compared with those of arc-melted bulk samples. The microstructure features and their influence on the martensitic transformation are analyzed. © 1999 Elsevier Science S.A. All rights reserved.

Keywords: Ti–Ni–Zr; Ti–Ni–Hf; Planar flow casting; Melt-spun ribbons; Microstructure; Mechanical properties

1. Introduction

Rapid quenching from the liquid phase (quenching rate varies from 10^4 up to 10^7 K/s) allows to obtain a material with an unusual structure and changed mechanical properties [1–11]. In melt-spun ribbons, the martensitic transformation temperatures are shifted with respect to the bulk material, the martensite plates have a specific morphology, and the functional properties are also changed as compared with those in bulk material. A large part of the experimental data concerning the study of a rapidly quenched ribbon structure has been obtained for the TiNi-based SMA's in which Cu (up to 25at.%) was added instead of Ni. There are several works related to the study of the parent and martensite phase structure in rapidly quenched TiNi-based alloys with addition of Cu and Co [1–11].

In this work the experimental results with respect to the structure and martensitic transformation parameters (temperatures and hysteresis loop) of the Ti–Ni–Zr and Ti–Ni–Hf melt-spun ribbons in comparison with the bulk material are presented. Ternary Ti–Ni–Zr and Ti–Ni–Hf shape memory alloys are known to be prospective materials for relatively high temperature applications, $T \geq 200$°C [12,13].

2. Material and experimental

The ingots of 50 g weight each have been elaborated by arc-melting under argon and annealed at 800°C for 10 h. The chemical composition was checked by X-ray fluorescence analysis. The ribbons were produced using an advanced variant of the single roller melt-spinning technique known as the planar flow casting. To get a ribbon which is not too brittle, free of cracks and holes, and having even a smooth surface, certain optimum conditions should be established. Melting and casting were performed in a helium atmosphere. A steel wheel of 20 cm diameter rotating at 1800 rot/min speed had been used. The melt temperature was the parameter mainly varied since it is related to the alloy liquidus temperature and affects strongly important properties of the melt such as its wetting on the substrate. The ejection pressure and wheel temperature were additional parameters helping to achieve the most appropriate casting conditions.

* Corresponding author. Tel./fax: +380-7-4442010.
E-mail address: kolomy@imp.kiev.ua (V. Kolomytsev)

0921-5093/99/$ - see front matter
PII: S0921-5093(99)00407-4

The chemical composition of the alloys and some selected parameters of the resulting good quality of the melt-spun ribbons obtained are presented in Tables 1 and 2. The phase composition of the ribbons at room temperature has been analyzed by X-ray diffraction (XRD) (Philips, Co–K_α). The measurements were carried out on both sides of the ribbons in order to have information from the regions related to different conditions of solidification.

The differential scanning calorimetry (DSC) technique has been applied to reveal martensitic and other phase transformations occurring in the alloys under investigation, and to determine their thermodynamic characteristics. A Mettler DSC30 calorimeter was used. Typical DSC curves obtained for Ti–Ni–Zr and Ti–Ni–Hf alloy samples are shown in Fig. 1. Calorimetric measurements were carried out both on bulk specimens and melt-spun ribbons to study the effect of rapid solidification. In order to control the stability of the martensitic transformation loop two thermal cycles for each experiment were made.

Functional properties, namely, the recoverable strain during the temperature cycling through the martensitic transformation temperature range as a function of applied load were studied in a unidirectional deformation mode on a specially designed dilatation-type-meter. The stress–strain–temperature dependencies obtained on the Ti–Ni–Hf ribbons are summarized in Figs. 3–5. The direct current heating of the sample has been used, and the sample temperature has been controlled by a thermocouple. The temperature stabilization and time variation of the sample were done automatically by a device consisting of the reference voltage generator, thermoelectric amplifier and temperature regulator. The sample loading system is based on the balance system in which one sample end was fixed and the other was attached to the balance support. The sample elongation and contraction during the load and temperature variation was checked by an induction receiver and amplifier. The analog signal output was also attached to the two-coordinator recorder input.

3. Results and discussion

In bulk, both ternary Ti–Ni–Zr and Ti–Ni–Hf alloys undergo a martensitic transformation at relatively high temperatures (Fig. 1). All as-melt-spun ribbons were crystalline with some uniformly distributed nanocrystalline component. In the ribbons, the martensitic transformation is suppressed and shifted to lower temperatures (see Fig. 1 and Table 2). For both alloy systems, the transformation sequence in bulk and ribbons is simple one stage transformation path on cooling and heating runs.

By means of the XRD-technique, the crystal structure of the as-received Ti–Ni–Zr ribbons at room temperature was found to be practically pure β-phase-b.c.c. B2-type ordered structure, while a mixture of the b.c.c. B2-type ordered parent and B19′ martensite phases was observed in samples cooled to liquid nitrogen temperature. A strong intensity of the $(110)_\beta$ X-ray line in comparison to the much lower intensity of other lines give evidence about the developed crystallization texture in the ribbons. After melt-spinning, the Ti–Ni–Hf ribbons were found to be a mixture of the b.c.c. B2-type ordered parent and the B19 martensite phases. No additional martensite was formed on cooling to

Table 1
Composition and physical properties of the melt-spun ribbons

Composition (at. %)		Liquidus temperature (°C)	Thickness (μm)	Yield strength (MPa)	Fracture stress (MPa)
Nominal	Analysis				
32Ti–50Ni–18Zr	32.2Ti–51.1Ni–16.7Zr	1308	33 ± 3	210 ± 20	510 ± 30
32Ti–50Ni–18Hf	32.2Ti–50.0Ni–17.7Hf	1312	35 ± 3	225 ± 20	240 ± 20

Table 2
Characteristic temperatures and enthalpy of the forward and reverse martensitic transformations (DSC data)

Alloy	Sample	M_s (°C)	M_f (°C)	ΔH_M (J/g)	A_s (°C)	A_f (°C)	ΔH_M (J/g)
Ti–Ni–Zr	Bulk	128	99	19.6	139	159	21.4
	Ribbon	−7	−41	7.1	14	43	9.3
Ti–Ni–Hf	Bulk	226	195	27.0	232	263	26.6
	Ribbon	157	132	20.2	175	199	21.6

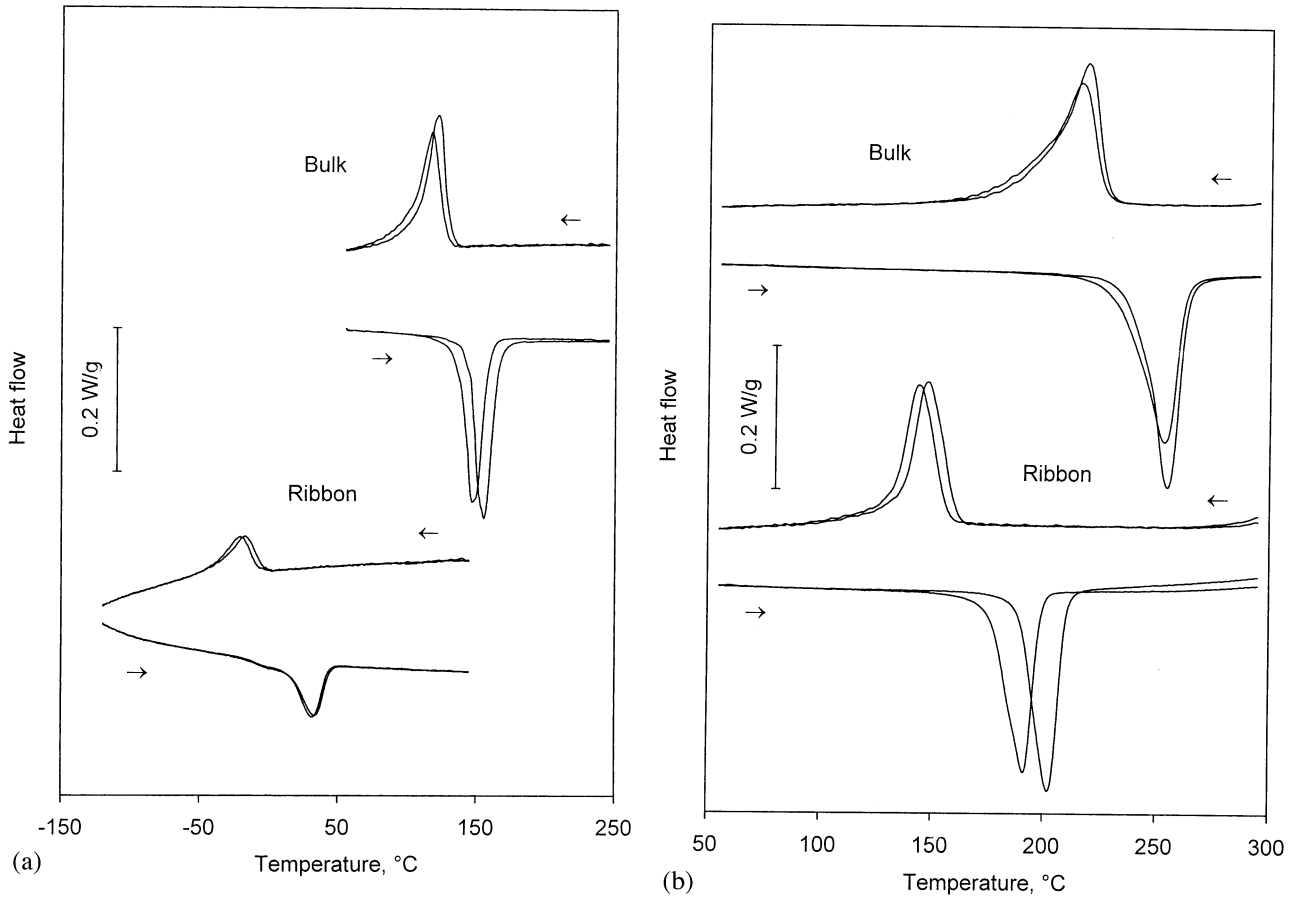

Fig. 1. Calorimetric data for the bulk and ribbon samples of Ti–Ni–Zr (a) and Ti–Ni–Hf (b) alloys for the first (left curves) and second transformation cycles.

liquid nitrogen temperature. It means that some part of the Ti–Ni–Hf ribbon is stabilized with respect to the martensitic transformation. Perhaps a similar situation is true for Ti–Ni–Zr ribbons.

The ribbon microstructure of ternary Ti–Ni–Zr and Ti–Ni–Hf alloys has been studied by means of the transmission electron microscopy (TEM) and selected area diffraction technique. The microstructure of both alloys was found to be a uniform mixture of the β-phase grains, martensite and nanocrystalline components. The β-phase grain size distribution function seems to be very disperse monomodal around 2 μm. In the Ti–Ni–Zr ribbons (according to DSC: $M_s = -7$°C; $M_f = -41$°C; $A_s = +14$°C; $A_f = +43$°C), the B2-ordered structure of wavy contrast caused by something like anti-phase domains decorated by chains of small particles was observed. The fine particles are uniformly distributed in the matrix and thought to be similar to $(TiZr)_2Ni$ type particles observed in bulk material. The martensite is a slightly monoclinic distorted 2H-type structure similar to that observed in bulk material. The martensite morphology is very disperse: martensite plates with 'rough boundaries' (Fig. 2a), with straight boundaries and a stacking fault substructure (Fig. 2b) are given. The martensite plates were usually observed near holes in twinned position, their size varies from less than 0.05 μm thickness and ~1 μm length. Perhaps stress relaxation near holes leads to a lower monoclinic angle. In the Ti–Ni–Hf ribbons (DSC: $M_s = +157$°C; $M_f = +132$°C; $A_s = +175$°C; $A_f = +199$°C), in martensite-free areas the microstructure similar to that observed in Ti–Ni–Zr ribbons is seen on some microstructure images, namely, the B2-ordered structure of wavy contract caused by something like anti-phase domains decorated by chain of small particles, which are believed to be $(TiHf)_2Ni$ particles (Fig. 2c, d). The martensite appears mostly in self-accommodated twinned plate-like form with twinning planes near $(111)_m$ and $(011)_m$. The width of individual plates varies from less than 0.05 μm to 1 μm, the length varies from ~0.15 μm to >1–2 μm; inside each plate smaller twins of the same variant system are usually observed; somewhere well-developed stacking faults along $(001)_m$ are also seen; the martensite crystal structure seems to be 2H modulated structure with orthorhombic lattice.

In bulk Ti–Ni–Zr and Ti–Ni–Hf alloys, the β-phase grain size is more than 10 μm, grains have a polyhedron shape in the as-cast ingot. The $(TiZr)_2Ni$ or $(TiHf)_2Ni$

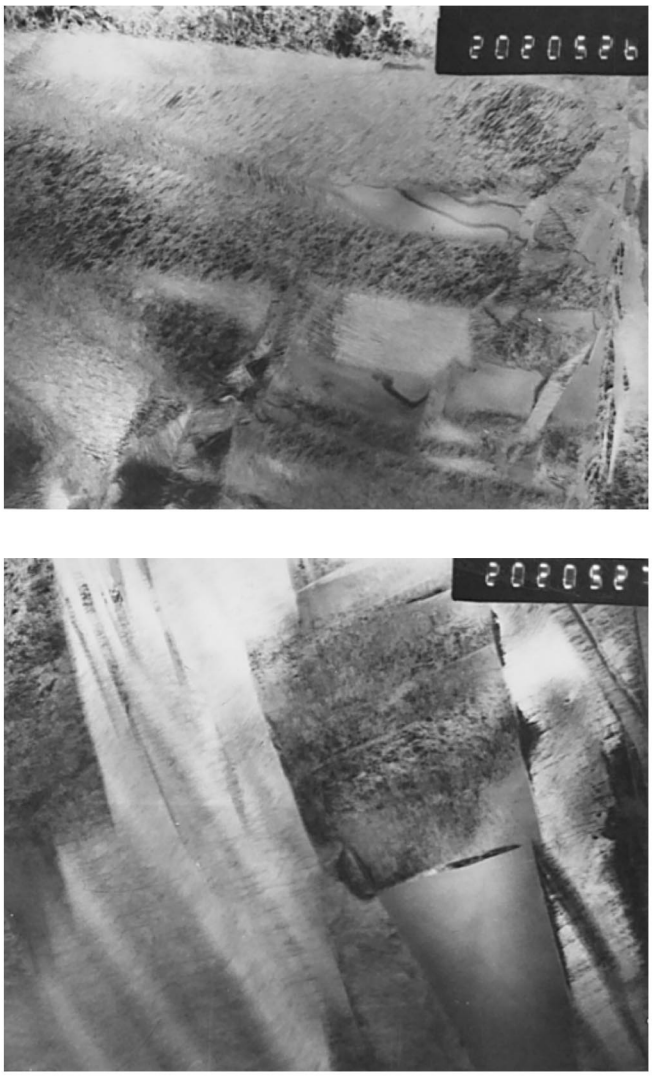

Fig. 2. Typical martensite microstructure of the Ti–Ni–Zr ribbons: (a) 'rough boundary' microstructure and (b) straight boundary and stacking fault substructure. Typical β-phase microstructure of the Ti–Ni–Hf ribbons: (c) wavy-like microstructure and fine precipitates and (d) SAD pattern form the area in (c).

type particles, respectively, are observed on a different scale, their size varied in a wide range from several nm up to approimately a few μm. For large particles, usually there is no relationship between the crystal lattices of the β-matrix and the precipitate, only very small particles are coherent with the matrix. It is known that the effect of precipitates on the martensite transformation temperatures and martensite structure is not unique and various possibilities are expected as a function of the nucleation and growth mechanisms, as it was found in the case of small coherent precipitates in TiNi-based alloys [14–17], Fe–Ni-based alloys [18], Cu–Al–X (X = Zn, Ni, Nb) [17,19].

Thus, contrary to bulk material, in ribbons the crystallization rate from the liquid solution at $T > 1300$°C is very high and a fine morphology and microstructure is formed as a mixture of the crystalline, nanocrystalline, martensite and small precipitate components. The particles are coherent or semicoherent with the matrix. Moreover, the microstructure of both alloy system ribbons is initially highly non-homogeneous and only some restricted material volume undergoes the martensitic transformation and contributes to the associated functional properties.

Thus, among the reasons for the decrease of the martensitic transformation temperatures in ribbons in comparison with bulk material, the following should be considered: a high density of grain boundaries of the components in their microstructure mixture which strongly resist the martensitic transformation; quenching stresses during rapid solidification which lower the temperature range of the B2 ⇒ B19′ and B2 ⇒ B19 martensitic transformations; loss of titanium or its chemical analogs Zr and Hf during tempering of the liquid solution prior to the ribbon production; precipitation or dissolution of secondary particles like $(TiZr)_2Ni$ and $(TiHf)_2Ni$ type particles or $(TiMe)_4Ni_2X$ type particles stabilized by X = O,S,P,C.

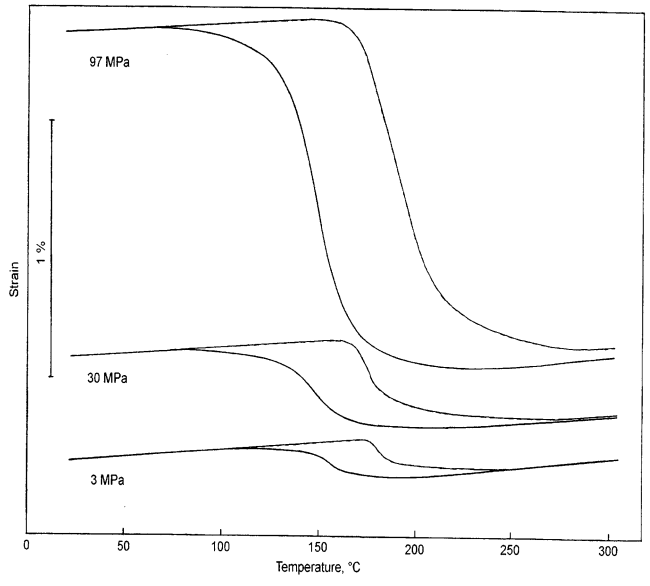

Fig. 3. The martensitic strain vs. temperature loops for different loads for the Ti–Ni–Hf ribbons.

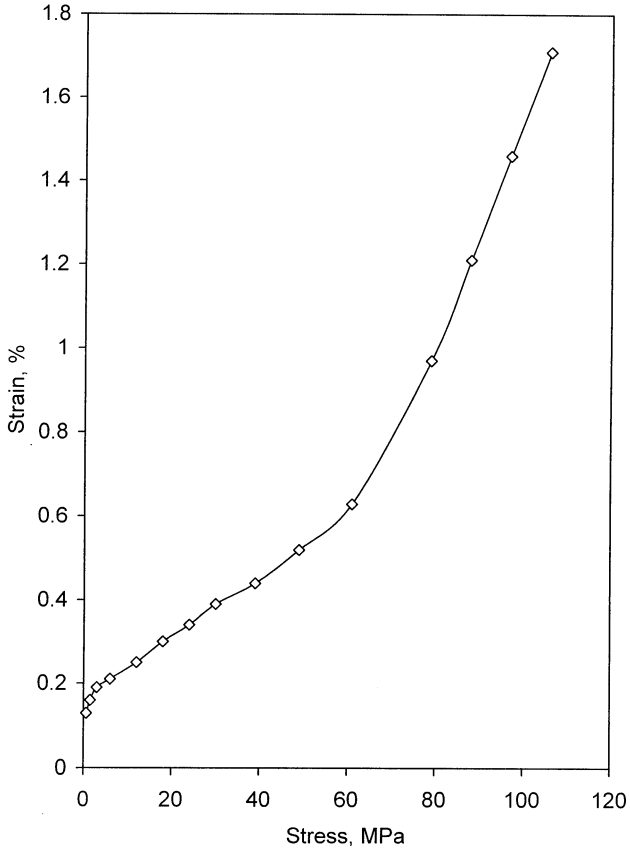

Fig. 4. Dependence of the maximal martensitic strain on the applied stress for the Ti–Ni–Hf ribbons.

The complex alloy microstructure mentioned above is reflected in the mechanical properties of the specimen. Despite a close similarity in the two ternary alloy microstructures, the elongation measured in the tensile test at room temperature differs very strongly for the two alloy systems — ~15% in Ti–Ni–Zr ribbons and <2% for Ti–Ni–Hf ribbons. The yield stress in both alloys is similar (see Table 1), while Ti–Ni–Hf ribbons are very brittle and their fracture stress is less than twice than that in Ti–Ni–Zr ribbons. Some difference in the elongation, the yield and fracture stresses is expected from the chemical composition considerations and from the different initial structure conditions — in Ti–Ni–Hf, the mixture of the parent and martensitic phases and in Ti–Ni–Zr a parent phase is close to the martensitic transformation temperature. Nevertheless, the high brittleness of the Ti–Ni–Hf alloy is an unwanted feature, and production conditions should be corrected taking into account its possible cause.

Unidirectional tensile tests have been used to study the mechanical behaviour of the ribbons in the martensitic transformation onset. The mechanical behaviour of

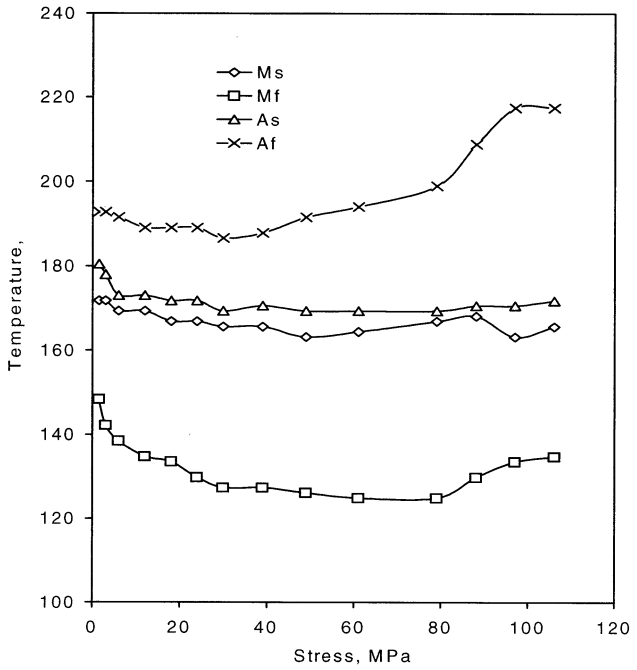

Fig. 5. Dependence of the characteristic martensitic transformation temperatures on the applied stress for the Ti–Ni–Hf ribbons.

the Ti–Ni–Hf ribbons was studied more carefully due to experimental convenience: high transformation temperatures allowed to use the direct current heating and air cooling of the sample. The specimen was heated to a temperature slightly above the finish reverse martensitic transformation temperature, loaded by various weights. Then the non-linear transformation strain and recovery strain were studied during thermal cycles as a function of the applied load. The results are summarized in Figs. 3–5. A non-linear dependence between the strain accumulated in the material during the martensitic transformation on cooling and the applied load was found (Fig. 4). A relatively weak response of the M_s and A_f transformation temperatures on the applied stress was detected (Fig. 5). Moreover, the M_s and A_s temperatures decrease with load, therefore, increasing their shift takes place in an opposite direction from that expected. It seems reasonable to suppose that such a behaviour is caused by a large ratio of the non-transforming part of the material which screens the influence of an applied load.

4. Conclusions

The Ti–Ni–Zr and Ti–Ni–Hf ribbons were produced using an advanced variant of the single roller melt-spinning technique known as the planar flow casting, which enabled to obtain rather wide ribbons of good quality. However, to get a non brittle ribbon being, free of cracks and holes, with an even and smooth surface, certain optimum conditions should be established and corrected.

In Ti–Ni–Zr and Ti–Ni–Hf shape memory alloys, the characteristic transformation temperatures are strongly influenced by the ribbon microstructure. A higher solubility of the alloying components, a higher level of quenched stresses, of coherent precipitates, fine β-phase grains — all these factors cause a decrease of the martensitic transformation temperatures in ribbons in comparison with bulk material.

Despite the close similarity in ribbon microstructure of the two alloy systems their mechanical and functional properties differ strongly, namely, the yield stress, the fracture stress and elongation in the Ti–Ni–Zr ribbons are better from a practical point of view than in Ti–Ni–Hf ribbons. Nevertheless, almost 2% of recoverable strain has been obtained for Ti–Ni–Hf ribbons at relatively high temperatures. Future improvement of the functional parameters for the Ti–Ni–Hf ribbons is expected by alloying and ageing treatment.

Acknowledgements

The financial support by INCO-Copernicus project IC15-CT96-0704 and Science and Technology Center in Ukraine project STCU-453 is thankfully acknowledged.

References

[1] N.M. Matveeva, Yu.K. Kovnerystii, L.A. Matlakhova, Z.G. Friedman, N.A. Lobsov, Izvestiya Acad. Sci. USSR, Metals 4 (1987) 97–100.
[2] N.M. Matveeva, Yu.K. Kovnerystii, Yu.A. Bykovskii, A.V. Shelyakov, O.V. Kostyanaya, Izvestiya Acad. Sci. USSR, Metals 4 (1989) 171–175.
[3] N.M. Matveeva, V.A. Lobodyuk, V.I. Kolomytsev, I.D. Lovzova, Izvestiya Acad. Sci. USSR, Metals 3 (1991) 164–168.
[4] M.B. Babanly, V.A. Lobodyuk, N.M. Matveeva, Peculiarities of martensite transformations in rapidly quenched 50Ti(50 − x)NixCu alloys, Proc. Martensite-91, Kiev, 1992, pp. 338–341.
[5] M.B. Babanly, V.A. Lobodyuk, N.M. Matveeva, Izvestiya Acad. Sci. USSR, Metals 5 (1993) 171–177.
[6] S. Eucken, E. Hornbogen, On martensite temperatures of rapidly quenched shape memory alloys, ICOMAT-86, Japan Institute of Metals, 1986, pp. 780–785.
[7] S.V. Mizin, A.I. Novikov, L.P. Fattkulina, Fizika Metall. Materialovedenie 9 (1990) 150–157.
[8] N. Matveeva, V. Pushin, A. Shelyakov, Y. Bykovskii, S. Volkova, V. Kraposhin, Phys. Metals Mater. Sci. 83 (3) (1997) 82.
[9] V. Pushin, S. Volkova, N. Matveeva, Phys. Metals Mater. Sci. 83 (4) (1997) 155.
[10] E. Cesari, J. Van Humbeeck, V. Kolomytsev, V. Lobodyuk, N. Matveeva, J. Phys. (France) IV 7 (1997) C5–C197.
[11] M. Larnicol, R. Portier, P. Ochin, J.Phys. (France) IV 7 (1997) C5–C191.

[12] W. Moorleghem, The investigation of new Ni–Ti shape memory alloys with emphasis on their application, PhD thesis, Institute of Metal Physics, Kiev, 1993, 152 p.
[13] V. Kolomytsev, Scripta Metall. 31 (10) (1994) 1415.
[14] V. Kolomytsev, M. Musienko, in: H. Morawiec, D. Stróż (Eds.), Precipitation Processes in TiNi-based SMA's, Proceedings of the XVI Conference of Applied Crystallography, Word Scientific, Singapore, 1995, pp. 234–241.
[15] V.M. Ermakov, V.I. Kolomytsev, V.A. Lobodyuk, L.G. Khandros, MITOM 5 (1981) 57–59.
[16] V.M. Ermakov, V.I. Kolomytsev, V.A. Lobodyuk, R.Ya. Musienko, MITOM 9 (1989) 61–64.
[17] L. Bataillard, R. Gotthardt, J. Phys. (France) IV 5 (1995) C8–C647.
[18] Yu. Koval, G. Monastyrskii, J. Phys. (France) IV 5 (1995) C8–C397.
[19] J. Lelatko, H. Morawiec, J. Mater. Sci. 31 (1996) 2767.